

Measurement of Exclusive Branching Fractions of Hadronic One-Prong Tau Decays

The L3 Collaboration

Abstract

We have measured the branching fractions for the hadronic τ decays, $\tau \rightarrow \pi/K n\pi^0 \nu$ ($0 \leq n \leq 3$), with the L3 detector at LEP. Multiphoton final states are analyzed using the fine-grained, high-resolution electromagnetic calorimeter. The decay channels are identified using a neural network method. The results are: $\text{BR}(\tau \rightarrow \pi/K \nu) = (11.82 \pm 0.26 \pm 0.43)\%$, $\text{BR}(\tau \rightarrow \pi/K \pi^0 \nu) = (25.05 \pm 0.35 \pm 0.50)\%$, $\text{BR}(\tau \rightarrow \pi/K 2\pi^0 \nu) = (8.88 \pm 0.37 \pm 0.42)\%$, $\text{BR}(\tau \rightarrow \pi/K 3\pi^0 \nu) = (1.70 \pm 0.24 \pm 0.38)\%$, where the first error quoted is statistical, the second systematic.

(Submitted to *Physics Letters B*)

Introduction

Twenty years after the discovery of the τ lepton [1] the τ hadronic decay modes and branching ratios are still a subject of debate [2]. It is not clear whether all hadronic τ decays have actually been observed experimentally or whether the measured branching fractions leave room for decay modes not predicted by the standard model. In addition, the measurements of τ hadronic branching ratios constitute important tests for some theoretical calculations [3].

The high center of mass energy of LEP facilitates the selection of τ -pair events and the rejection of background from hadron events. In addition, the high luminosity of LEP and the large τ -pair production cross section at the Z pole provide high statistics. In particular, the high resolution and fine granularity of the L3 electromagnetic calorimeter allows a clean separation and analysis of decay modes with one or more neutral pions.

In this study, we present results for hadronic τ decays into a single charged particle, h (π^\pm or K^\pm), plus n π^0 , where ($0 \leq n \leq 3$). We use data collected with the L3 detector at LEP in the 1992 running period. The sample corresponds to an integrated luminosity of 21.68 pb $^{-1}$ after restriction to periods where all relevant parts of the detector and triggers were active.

The L3 detector

The L3 detector is designed to measure electrons, photons, muons and jets produced in e^+e^- reactions with good spatial and energy resolution. Starting from the interaction point, the L3 detector is composed of the following sub-detectors: a central tracking chamber ($13^\circ < \theta < 167^\circ$) consisting of a time expansion chamber (TEC) and z-chambers; a fine-grained electromagnetic calorimeter (ECAL) consisting of a barrel ($42^\circ < \theta < 138^\circ$) and endcaps ($10^\circ < \theta < 37^\circ$ and $143^\circ < \theta < 170^\circ$), composed of Bismuth Germanium Oxide crystals; a hadron calorimeter (HCAL) with uranium absorber and proportional wire chambers ($5^\circ < \theta < 175^\circ$); a muon spectrometer (MUCH) consisting of multi-wire drift chambers ($35.8^\circ < \theta < 144.2^\circ$). These detectors are installed in a 12 m inner diameter solenoidal magnet which provides a uniform magnetic field of 0.5 T along the beam direction. A detailed description of the detector and its performance is given in ref. [4].

Selection of one-prong tau decays

The analysis is restricted to the barrel part of the detector, which has an acceptance of $|\cos\theta| < 0.7$, where θ is the polar angle of the thrust axis of the event. We require that the polar angles of the thrust axis of the two jets from both tau decays must be in the fiducial region. A Monte Carlo calculation gives a geometrical acceptance of 57.8 % in the fiducial region. The $\tau^+\tau^-$ events are generated with the KORALZ program, version 3.8 [5], with full simulation of the L3 detector response [6]. The simulation uses the default KORALZ branching fractions. The reaction $e^+e^- \rightarrow \tau^+\tau^-$ is identified by selecting low-multiplicity final states in the central tracking chamber as well as the calorimeters, following the preselection of Ref. [7]. Other low-multiplicity reactions are then rejected as follows:

- $e^+e^- \rightarrow e^+e^-$ are rejected by requiring the total energy in the electromagnetic calorimeter to be smaller than 65 GeV and the energies of the two most energetic clusters to be both smaller than 40 GeV.

- $e^+e^- \rightarrow \mu^+\mu^-$ are rejected if one hemisphere of the event has a muon identified in the muon detector as well as a minimum ionizing signature in the calorimeters and the other hemisphere has a muon candidate.
- Final states from two-photon reactions are rejected by requiring a minimum total calorimetric energy of 13 GeV.

Every τ -pair event is then divided into two hemispheres by the plane perpendicular to the thrust axis of the event. Each τ -decay hemisphere is now considered separately. In a hemisphere, we require exactly one charged particle which is well measured by the central tracking chamber in both the $r\phi$ and z projections. The Monte Carlo simulation of the efficiency of the central tracking chamber was checked using data samples of $e^+e^- \rightarrow e^+e^-$ and $\mu^+\mu^-$ events.

The selection efficiency of one-prong tau decays is 67.3% within the fiducial region. After this selection, we are left with 24776 decays. The sample purity is $(97.2 \pm 0.1)\%$; the main backgrounds are: $(1.5 \pm 0.1)\%$ from $\mu^+\mu^-$ final states, and $(1.2 \pm 0.1)\%$ from e^+e^- final states. The backgrounds from the two-photon reactions are negligible.

Selection of one-prong hadronic tau decays

The charged particle is required to be inconsistent with a reconstructed muon (defined as a track in the muon detector accompanied by a minimum ionizing signature in the calorimeters). We reject electrons by requiring that the shower profile of the charged particle be inconsistent with that of an electromagnetic shower. The shower left by the tau decay in the electromagnetic calorimeter is then analyzed as a single charged hadron and a variable number of neutral clusters. For this purpose, we use the average transverse profile of hadronic and electromagnetic showers in the electromagnetic calorimeter as a function of energy and impact point [7] determined using a combination of L3 data and test beam data. First, the average hadronic shower energy is subtracted from each crystal in the jet from tau decay, as predicted on the basis of the impact point extrapolated from the central tracking chamber and the energy measured in the impacted crystal. Each local maximum in the remaining shower is then identified as a neutral cluster whose shower has a profile predicted by the L3 data and whose energy corresponds to that of the local maxima. Leakage from electromagnetic showers into hadronic showers and vice versa is then recalculated. The procedure is iterated, varying the energies and centers of the shower components, until the energies and centers of the shower components stabilize to an optimum description of the calorimetric objects in the hemisphere. Usually, the algorithm converges after 3 to 4 iterations. The neutral clusters in a tau decay are then ordered by decreasing energy. The minimum energy requirements (E_n) for neutral clusters are between 400 MeV and 500 MeV depending on the number of neutral clusters. The distribution of the numbers of hadronic one-prong tau decays as a function of the number of neutral clusters detected is shown in Fig. 1. The branching fractions from the final fit in this measurement were used in the figure. We observe good agreement between data and Monte Carlo.

After rejecting electrons and muons in τ decays, we find 2829 decays with no neutral clusters, 6526 with one neutral cluster, 3769 with two neutral clusters, 1034 with three neutral clusters, 309 with four neutral clusters and 97 with five neutral clusters. The decays containing one or more neutral clusters are subjected to analysis using neural networks below.

Decays without neutral clusters

When no neutral cluster is found in the hemisphere, we apply more stringent criteria to reject leptonic final states. The longitudinal and transverse shower profiles in the calorimeters are required to be incompatible with those of an electron or minimum ionizing particle. In addition, the energy transverse to the charged particle direction in the electromagnetic calorimeter is limited to eliminate accompanying electromagnetic showers.

Decays with one or more neutral clusters

The analysis of the decay modes with one or more neutral clusters was carried out using a feed-forward neural network [8]. Back-propagation was used for training the networks [9]. There is a network for each combination of number of observed neutral clusters and number of generated neutral particles. All neural networks have three layers: one input layer, one hidden layer, and one output layer. The networks have 17, 18, 21 and 22 input variables for $n = 1, 2, 3$ and 4 reconstructed neutral clusters, respectively. The hidden layers have the same number of nodes as the input layer. Each output layer has only one node, the output of which determines whether or not the decay is selected for a particular decay channel.

As examples of the neural network input, Fig. 2 shows the distributions in the energy of the charged particle, the neutral particles and the energy in the electromagnetic calorimeter transverse to the charged particle direction. Fig. 3 shows the distributions of the angles between charged hadron and neutral clusters, as well as the angle between the neutral clusters in the sample $h 2\pi^\circ$. Also shown in the two figures are the contributions to these distributions from the decay channels under study and the background as predicted by the Monte Carlo after adjustment of the branching fractions to our final results. The Monte Carlo description of details of the shower shape is in good agreement with data. Each of the networks is then trained on a Monte Carlo sample of known τ -decay channels. The training sample of 250 000 $\tau^+\tau^-$ events is generated with the KORALZ program.

The data sample is then subjected to selection and rejection by the networks using the training relevant to the signal and major background channels. A hemisphere is classified into a signal channel if it is selected by only one network. Hemispheres that are not selected by any network are rejected.

Results

The background from τ decays into $\pi K_L^0 \nu$ in the selected sample of $h\nu$ (with one neutral or without neutrals) is suppressed by requiring the ratio of the energy deposited in the calorimeters to the momentum measured in TEC to be less than 2.8. Thus we select 2967, 6613, 1060 and 293 decays in the four decay channels h , $h \pi^\circ$, $h 2\pi^\circ$ and $h 3\pi^\circ$ respectively. The distribution of the total hadronic invariant mass in the last three categories is shown in Fig. 4 together with the respective Monte Carlo result for signal and background after adjustment of our final branching fractions. The slight shift in the mass spectra in Figs. 4b-c may indicate small defects in the simulation. These deviations are small and their influence on the detection efficiencies has been included in the systematic errors.

The selection efficiency of an event with a given number of neutral clusters into one of the decay channels is determined by applying the selection procedure to a Monte Carlo sample of 110 000 $\tau^+\tau^-$ events which is independent of the sample used for training. The efficiencies are

Source	Selection Efficiency (%)			
	h	h π°	h $2\pi^\circ$	h $3\pi^\circ$
$\pi/K \nu$	56.56	3.33	0.30	0.03
$\pi/K \pi^\circ \nu$	2.50	65.09	1.23	0.15
$\pi/K 2\pi^\circ \nu$	0.24	9.73	26.14	3.78
$\pi/K 3\pi^\circ \nu$	0.09	2.09	9.22	21.28
$\pi/K 4\pi^\circ \nu$	–	0.71	3.00	20.20
$\pi/K \eta\pi^\circ \nu$	–	1.20	3.40	15.60
$\pi K_L^0 \nu$	27.36	17.72	0.84	0.18
$e \nu \nu$	0.98	0.79	0.21	–
$\mu \nu \nu$	0.80	0.61	0.02	–
3-prong	0.08	0.21	0.06	–
$e^+ e^-$	0.03	0.004	–	–
$\mu^+ \mu^-$	0.26	0.04	–	–

Table 1: Efficiencies to select a given final state in each of the four experimental categories. These efficiencies are calculated within the fiducial region by Monte Carlo on a test sample of events.

shown in Table 1. The efficiencies include both the efficiencies in the $\tau^+\tau^-$ event selection and the efficiencies in the decay mode identification by the neural network method. The probabilities to accept an event from the two main background sources are also shown.

Determination of branching fractions

Branching fractions are determined using the relation

$$N_i^{\text{exp}} = N_\tau \sum_{j=1,10} \text{BR}_j \epsilon_j^i + \sum_{k=1,2} N_k^{\text{bg}} \epsilon_k^i \quad (1)$$

N_i^{exp} is the number of events expected in an decay channel i , N_τ is the total number of τ decays, calculated from the integrated luminosity and measured $\tau^+\tau^-$ cross section from the L3 experiment in the fiducial region [10]. N_k^{bg} is the number of background events. The branching fractions BR_j are determined using a χ^2 fit which compares the predicted number and the observed number of decays in the four decay channels. No constraint is used on the sum of the branching fractions. The index i runs over the number of neutral clusters, j over the ten τ decay channels considered as specified in Table 1 and k over the main background channels. ϵ_j^i is the detection efficiency for an event with i observed neutral clusters which results from a decay with j generated neutral particles as specified in Table 1. The results are:

$$\begin{aligned} \text{BR}(\pi/K \nu) &= (11.82 \pm 0.26 \pm 0.43)\% \\ \text{BR}(\pi/K \pi^\circ \nu) &= (25.05 \pm 0.35 \pm 0.50)\% \\ \text{BR}(\pi/K 2\pi^\circ \nu) &= (8.88 \pm 0.37 \pm 0.42)\% \\ \text{BR}(\pi/K 3\pi^\circ \nu) &= (1.70 \pm 0.24 \pm 0.38)\% \end{aligned}$$

The first error quoted is statistical, the second systematic. The correlation matrix from the fit is listed in Table 2.

	h	h π°	h $2\pi^\circ$	h $3\pi^\circ$
h	1.00	-0.11	0.00	0.00
h π°	-0.11	1.00	-0.19	0.06
h $2\pi^\circ$	0.00	-0.19	1.00	-0.48
h $3\pi^\circ$	0.00	0.06	0.48	1.00

Table 2: The correlation matrix of the fit.

Contributions to the systematic error for each decay channel are listed in Table 3. The systematic uncertainties in the $\tau^+\tau^-$ selection for each decay channel are listed in first row. The contribution from the normalization uncertainty are listed in the second row. We estimate uncertainties in the selection of $\tau^+\tau^-$ events by varying the primary selection cuts by $\pm 10\%$ and taking the maximum observed change in the branching fraction as the contribution to the systematic error. The only exception is the cut in the energy of electromagnetic clusters which is varied by 5%. Since all branching fractions are determined by normalizing to the total number of produced $\tau^+\tau^-$ final states, a normalization error arises from the uncertainty in the measured $\tau^+\tau^-$ total cross section (0.7%) and the luminosity (0.5%) [10].

Source	$\Delta\text{BR}(\pi/K \nu)$	$\Delta\text{BR}(\pi/K \pi^\circ \nu)$	$\Delta\text{BR}(\pi/K 2\pi^\circ \nu)$	$\Delta\text{BR}(\pi/K 3\pi^\circ \nu)$
$\tau\tau$ selection	0.14	0.20	0.11	0.17
N_τ	0.10	0.22	0.08	0.02
MC statistics	0.18	0.26	0.18	0.15
E_n threshold	0.03	0.07	0.07	0.10
NN output	0.04	0.13	0.22	0.18
NN input	0.29	0.28	0.22	0.20
h selection cuts	0.16	-	-	-
Form factor	-	-	0.18	0.09
h $4\pi^\circ$	-	-	0.02	0.06
h $\eta \pi^\circ$	-	-	0.01	0.02
$\pi K_L^0 \nu$	0.08	0.03	0.01	-
Total	0.43	0.50	0.42	0.38

Table 3: Breakdown of the systematic error (in %) on the four measured branching fractions. The sources of systematic error are explained in the text.

The dominant contribution to the systematic error comes from the procedure identifying the final states and from the efficiency determination. The first part in this error is taken from the statistical uncertainties of the efficiencies predicted by Monte Carlo. The energy cuts E_n on neutral clusters were varied by $\pm 10\%$ to estimate the systematic uncertainty. More important is the systematic uncertainty due to the neural network selection. We estimate this first by varying the cut on each neural network's output by 10%. In addition, we identify the input variables which have the largest influence on the networks' decisions by applying a shift or a scale factor to the inputs one by one. This variation is applied to the inputs from the data only, while the network training and the Monte Carlo inputs stay constant. By observing the systematic changes in the extracted branching fractions, we find that the momentum, electromagnetic and

hadronic energies and the transverse electromagnetic energy, as well as the energies and angles of the three most energetic neutral clusters (via the reconstructed invariant masses used as inputs) have the largest influence on the result. We determine the allowed shifts and scale factors of these inputs by calculating the χ^2 of the fit of the experimental distribution to the corresponding Monte Carlo prediction. A $\Delta\chi^2$ of one between the optimum shift and scale and the maximum allowed shift gives the errors quoted in Table 3. For events with no neutral clusters which were not subject to network selection, we estimate the error on the selection efficiency by varying all cuts by $\pm 10\%$ and assigning the largest deviation observed.

In addition, the D-wave contribution to the a_1 amplitude and the ρ substructure of the $\pi/K 3\pi^0 \nu$ modes are not modeled correctly by the Monte Carlo event generation which could lead to small errors in the calculated selection efficiency by changing the correlations between the network input variables. The ratio of D- to S-wave amplitudes has been measured by ARGUS [11] to be -0.11 ± 0.02 and we estimate this could lead to a maximum of a 2% error in the selection efficiency calculation for the $\pi/K 2\pi^0 \nu$ mode. This error also includes any contribution from other resonant substructure. The presence of ρ substructure in the $\pi/K 3\pi^0 \nu$ mode has also been measured by ARGUS [12] and we estimate the largest error from this source to be 5%. Both of these errors have been included in the systematic errors.

A final type of error arises from the decay channels πK_L^0 , $h 4\pi^0$ and $h \eta \pi^0$, where η decays into neutrals. We take the inclusive branching fraction into πK^0 of 1.3% from the HRS measurement [14], and assume that 50% of the K^0 are K_L^0 . We assign the branching fractions into $h 4\pi^0$ and $h \eta \pi^0$ to those measured by the CLEO experiment [15, 16]. We take the measurement errors to estimate our systematic errors.

As an independent cross-check on the analysis technique, a separate analysis [13] was performed using cuts in the quantities with most separation power between channels. The results are consistent with the values obtained by the neural network method.

Conclusions

The branching fractions for the hadronic τ decays, $\tau \rightarrow \pi/K n\pi^0 \nu$ with n between zero and three, have been measured with the L3 detector at LEP. Multiphoton final states are identified by a neural network method. The results are:

$$\begin{aligned} \text{BR}(\pi/K \nu) &= (11.82 \pm 0.26 \pm 0.43)\% \\ \text{BR}(\pi/K \pi^0 \nu) &= (25.05 \pm 0.35 \pm 0.50)\% \\ \text{BR}(\pi/K 2\pi^0 \nu) &= (8.88 \pm 0.37 \pm 0.42)\% \\ \text{BR}(\pi/K 3\pi^0 \nu) &= (1.70 \pm 0.24 \pm 0.38)\% \end{aligned}$$

These results are in agreement with the current world averages [17]. They also agree with more recent determinations from OPAL [18] and CLEO [15].

Acknowledgments

We wish to express our gratitude to the CERN accelerator divisions for the excellent performance of the LEP machine. We acknowledge the efforts of all engineers and technicians who have participated in the construction and maintenance of this experiment.

The L3 Collaboration:

M.Acciarri,²⁶ A.Adam,⁴³ O.Adriani,¹⁶ M.Aguilar-Benitez,²⁵ S.Ahlen,¹⁰ J.Alcaraz,²⁵ A.Aloisio,²⁸ G.Alverson,¹¹ M.G.Alvigi,²⁸ G.Ambrosi,³³ Q.An,¹⁸ H.Anderhub,⁴⁶ A.L.Anderson,¹⁵ V.P.Andreev,³⁷ T.Angelescu,¹² L.Antonov,⁴⁰ D.Antreasyan,⁸ G.Alkhadov,³⁷ P.Arce,²⁵ A.Arefiev,²⁷ T.Azemoon,³ T.Aziz,⁹ P.V.K.S.Baba,⁸ P.Bagnaia,^{36,17} J.A.Bakken,³⁵ L.Baksay,⁴² R.C.Ball,³ S.Banerjee,⁹ K.Banicz,⁴³ R.Barillere,¹⁷ L.Barone,³⁶ A.Baschiroto,²⁶ M.Basile,⁸ R.Battiston,³³ A.Bay,²² F.Becattini,¹⁶ U.Becker,¹⁵ F.Behner,⁴⁶ Gy.L.Bencze,¹³ J.Berdugo,²⁵ P.Berges,¹⁵ B.Bertucci,¹⁷ B.L.Betev,^{40,46} M.Biasini,³³ A.Biland,⁴⁶ G.M.Bilei,³³ R.Bizzarri,³⁶ J.J.Blaising,⁴ G.J.Bobbink,^{17,2} R.Bock,¹ A.Böhm,¹ B.Borgia,³⁶ A.Boucham,⁴ D.Bourilkov,⁴⁶ M.Bourquin,¹⁹ D.Boutigny,¹⁷ B.Bouwens,² E.Brambilla,¹⁵ J.G.Branson,³⁸ V.Brigljevic,⁴⁶ I.C.Brock,³⁴ M.Brooks,²³ A.Bujak,⁴³ J.D.Burger,¹⁵ W.J.Burger,¹⁹ C.Burgos,²⁵ J.Busenitz,⁴² A.Buytenhuijs,³⁰ A.Bykov,³⁷ X.D.Cai,¹⁸ M.Capell,¹⁵ G.Cara Romeo,⁸ M.Caria,³³ G.Carlino,²⁸ A.M.Cartacci,¹⁶ J.Casaus,²⁵ R.Castello,²⁶ N.Cavallo,²⁸ M.Cerrada,²⁵ F.Cesaroni,³⁶ M.Chamizo,²⁵ Y.H.Chang,⁴⁸ U.K.Chaturvedi,⁸ M.Chemarin,²⁴ A.Chen,⁴⁸ C.Chen,⁶ G.Chen,^{6,46} G.M.Chen,⁶ H.F.Chen,²⁰ H.S.Chen,⁶ M.Chen,¹⁵ G.Chiefari,²⁸ C.Y.Chien,⁵ M.T.Choi,⁴¹ S.Chung,¹⁵ L.Cifarelli,⁸ F.Cindolo,⁸ C.Civinini,¹⁶ I.Clare,¹⁵ R.Clare,¹⁵ T.E.Coan,²³ H.O.Cohn,³¹ G.Coignet,⁴ N.Colino,¹⁷ S.Costantini,³⁶ F.Cotorobai,² B.de la Cruz,²⁵ X.T.Cui,¹⁸ X.Y.Cui,¹⁸ T.S.Dai,¹⁵ R.D'Alessandro,¹⁶ R.de Asmundis,²⁸ A.Degré,⁴ K.Deiters,⁴⁴ E.Dénes,¹³ P.Denes,³⁵ F.DeNotaristefani,³⁶ D.DiBitonto,⁴² M.Diemoz,³⁶ H.R.Dimitrov,⁴⁰ C.Dionisi,³⁶ M.Dittmar,⁴⁶ L.Djambazov,⁴⁶ I.Dorne,⁴ M.T.Dova,^{18,4} E.Drago,²⁸ D.Duchesneau,¹⁷ F.Duhem,⁴ P.Duinker,¹ I.Duran,³⁹ S.Dutta,⁹ S.Easo,³³ H.El Mamouni,²⁴ A.Engler,³⁴ F.J.Eppling,¹⁵ F.C.Erné,^{2,17} P.Extermann,¹⁷ R.Fabbretti,⁴⁴ M.Fabre,⁴⁴ S.Falciano,³⁶ A.Favara,¹⁶ J.Fay,²⁴ M.Felcini,⁴⁶ T.Ferguson,³⁴ D.Fernandez,²⁵ G.Fernandez,²⁵ F.Ferroni,³⁶ H.Fesefeldt,¹ E.Fiandrini,³³ J.H.Field,¹⁹ F.Filthaut,³⁰ P.H.Fisher,⁵ G.Forconi,¹⁵ L.Fredj,¹⁹ K.Freudenreich,⁴⁶ M.Gaillard,²² Yu.Galakionov,^{27,15} E.Gallo,¹⁶ S.N.Ganguli,⁹ P.Garcia-Abia,²⁵ S.Gentile,³⁶ J.Gerald,¹⁵ N.Gheordanescu,¹² S.Giagu,³⁶ S.Goldfarb,²² J.Goldstein,¹⁰ Z.F.Gong,²⁰ E.Gonzalez,²⁵ A.Gougas,⁵ D.Goujon,¹⁹ G.Gratta,³² M.W.Gruenewald,⁷ C.Gu,¹⁸ M.Guanzirola,¹⁸ V.K.Gupta,³⁵ A.Gurtu,⁹ H.R.Gustafson,³ L.J.Gutay,⁴³ A.Hasan,²⁹ D.Hauschildt,² J.T.He,⁶ T.Hebbeker,⁷ M.Hebert,³⁸ A.Hervé,¹⁷ K.Hilgers,¹ H.Hofer,⁴⁶ H.Hoorani,⁹ S.R.Hou,⁴⁸ G.Hu,¹⁸ B.Ille,²⁴ M.M.Ilyas,¹⁸ V.Innocente,¹⁷ H.Janssen,⁴ B.N.Jin,⁶ L.W.Jones,³ P.de Jong,¹⁵ I.Josa-Mutuberria,¹⁷ A.Kasser,²² R.A.Khan,¹⁸ Yu.Kamyshkov,³¹ P.Kapinos,⁴⁵ J.S.Kapustinsky,²³ Y.Karyotakis,¹⁷ M.Kaur,¹⁸ S.Khokhar,¹⁸ M.N.Kienzle-Focacci,¹⁹ D.Kim,⁵ J.K.Kim,⁴¹ S.C.Kim,⁴¹ Y.G.Kim,⁴¹ W.W.Kinnison,²³ A.Kirkby,³² D.Kirkby,³² J.Kirkby,¹⁷ S.Kirsch,⁴⁵ W.Kittel,³⁰ A.Klimentov,^{15,27} A.C.König,³⁰ E.Koffeman,² O.Kornadt,¹ V.Koutsenko,^{15,27} A.Koulbardi,³⁷ R.W.Kraemer,³⁴ T.Kramer,¹⁵ V.R.Krastev,^{40,33} W.Krenz,¹⁴ H.Kuijten,³⁰ K.S.Kumar,¹⁴ A.Kunin,^{15,27} P.Ladron de Guevara,^{25,17} G.Landi,¹⁶ D.Lanske,¹ S.Lanzano,^{28,1} P.Laurikainen,²¹ A.Lebedev,¹⁵ P.Lebrun,²⁴ P.Lecomte,⁴⁶ P.Lecoq,¹⁷ P.Le Coultre,⁴⁶ D.M.Lee,²³ J.S.Lee,⁴¹ K.Y.Lee,⁴¹ I.Leedom,¹¹ C.Leggett,³ J.M.Le Goff,¹⁷ R.Leiste,⁴⁵ M.Lenti,¹⁶ E.Leonardi,³⁶ P.Levtchenko,³⁷ C.Li,^{20,18} E.Lieb,⁴⁵ W.T.Lin,⁴⁸ F.L.Linde,² B.Lindemann,¹ L.Lista,²⁸ Y.Liu,¹⁸ W.Lohmann,⁴⁵ E.Longo,³⁶ W.Lu,³⁶ Y.S.Lu,⁶ J.M.Lubbers,¹⁷ K.Lübelsmeyer,¹ C.Luci,³⁶ D.Luckey,¹⁵ L.Ludovici,³⁶ L.Luminari,³⁶ W.Lustermann,⁴⁴ W.G.Ma,²⁰ M.MacDermott,⁴⁶ M.Maity,⁹ L.Malgeri,³⁶ R.Malik,¹⁸ A.Malinin,²⁷ C.Maña,²⁵ S.Mangla,⁹ M.Maolinba,⁴⁶ P.Marchesini,⁴⁶ A.Marin,¹⁰ J.P.Martin,²⁴ F.Marzano,³⁶ G.G.G.Massaró,² K.Mazumdar,⁹ P.McBride,¹⁴ T.McMahon,⁴³ D.McNally,³⁸ S.Mele,²⁸ M.Merk,³⁴ L.Merola,²⁸ M.Meschini,¹⁶ W.J.Metzger,³⁰ Y.Mi,²² A.Mihul,¹² G.B.Mills,²³ Y.Mir,¹⁸ G.Mirabelli,³⁶ J.Mnich,¹ M.Möller,¹ V.Monaco,³⁶ B.Monteleoni,¹⁶ R.Morand,¹⁴ S.Morganti,³⁶ N.E.Moulai,¹⁸ R.Mount,³² S.Müller,¹ E.Nagy,¹³ M.Napolitano,²⁸ F.Nessi-Tedaldi,⁴⁶ H.Newman,³² M.A.Niaz,¹⁸ A.Nippe,¹ H.Nowak,⁴⁵ G.Organtini,³⁶ R.Ostenson,²¹ D.Pandoulas,¹ S.Paoletti,³⁶ P.Paolucci,²⁸ G.Pascale,³⁶ G.Passaleva,^{16,33} S.Patricelli,²⁸ T.Paul,⁵ M.Pauluzzi,³³ C.Paus,¹ F.Pauss,⁴⁶ Y.J.Pei,¹ S.Pensotti,²⁶ D.Perret-Gallix,⁴ A.Pevsner,⁵ D.Piccolo,²⁸ M.Pieri,¹⁶ J.C.Pinto,³⁴ P.A.Piroué,³⁵ E.Pistolessi,¹⁶ F.Plasil,³¹ V.Plyaskin,²⁷ M.Pohl,⁴⁶ V.Pojidaev,^{27,16} H.Postema,¹⁵ N.Produit,¹⁹ J.M.Qian,³ K.N.Qureshi,¹⁸ R.Raghavan,⁹ G.Rahal-Callot,⁴⁶ P.G.Rancoita,²⁶ M.Rattaggi,²⁶ G.Raven,² P.Razis,²⁹ K.Read,³¹ M.Redaeli,²⁶ D.Ren,⁴⁶ Z.Ren,¹⁸ M.Rescigno,³⁶ S.Reucroft,¹¹ A.Ricker,¹ S.Riemann,⁴⁵ B.C.Riemers,⁴³ K.Riles,³ O.Rind,³ H.A.Rizvi,¹⁸ S.Ro,⁴¹ A.Robohm,⁴⁶ F.J.Rodriguez,²⁵ B.P.Roe,³ M.Röhner,¹ S.Röhner,¹ L.Romero,²⁵ S.Rosier-Lees,⁴ R.Rosmalen,³⁰ Ph.Rosselet,²² W.van Rossum,² S.Roth,¹ A.Rubbia,¹⁵ J.A.Rubio,¹⁷ H.Rykaczewski,⁴⁶ J.Salicio,¹⁷ J.M.Salicio,²⁵ E.Sanchez,²⁵ G.S.Sanders,²³ A.Santocchia,³³ M.E.Sarakinos,⁴³ S.Sarkar,⁹ G.Sartorelli,¹⁸ M.Sassowsky,¹ G.Sauvage,⁴ C.Schäfer,¹ V.Schegelsky,³⁷ D.Schmitz,¹ P.Schmitz,¹ M.Schneegans,⁴ N.Scholz,⁴⁶ H.Schopper,⁴⁷ D.J.Schotanus,³⁰ S.Shotkin,¹⁵ H.J.Schreiber,⁴⁵ J.Shukla,³⁴ R.Schulte,¹ K.Schultze,¹ J.Schwenke,¹ G.Schwering,¹ C.Sciacca,²⁸ I.Scott,¹⁴ R.Sehgal,¹⁸ P.G.Seiler,⁴⁴ J.C.Sens,^{17,2} L.Servoli,³³ I.Sheer,³⁸ S.Shevchenko,³² X.R.Shi,³² E.Shumilov,²⁷ V.Shoutko,²⁷ D.Son,⁴¹ A.Sopczak,¹⁷ V.Soulimov,²⁸ C.Spartiotis,²¹ T.Spickermann,¹ P.Spillantini,¹⁶ M.Steuer,¹⁵ D.P.Stickland,³⁵ F.Sticozzi,¹⁵ H.Stone,³⁵ K.Strauch,¹⁴ K.Sudhakar,⁹ G.Sultanov,¹⁸ L.Z.Sun,^{20,18} G.F.Susinno,¹⁹ H.Suter,⁴⁶ J.D.Swain,¹⁸ A.A.Syed,³⁰ X.W.Tang,⁶ L.Taylor,¹¹ R.Timellini,⁸ Samuel C.C.Ting,¹⁵ S.M.Ting,¹⁵ O.Toker,³³ M.Tonutti,¹ S.C.Tonwar,⁹ J.Tóth,¹³ G.Trowitzsch,⁴⁵ A.Tsaregorodtsev,³⁷ G.Tsipolitis,³⁴ C.Tully,³⁵ J.Ulbricht,⁴⁶ L.Urbán,¹³ U.Uwer,¹ E.Valente,³⁶ R.T.Van de Walle,³⁰ I.Vetlitsky,²⁷ G.Viertel,⁴⁶ P.Vikas,¹⁸ U.Vikas,¹⁸ M.Vivargent,⁴ H.Vogel,³⁴ H.Vogt,⁴⁵ I.Vorobiev,^{14,27} A.A.Vorobyov,³⁷ An.A.Vorobyov,³⁷ L.Vuilleumier,²² M.Wadhwa,²⁵ W.Wallraff,¹ J.C.Wang,¹⁵ X.L.Wang,²⁰ Y.F.Wang,¹⁵ Z.M.Wang,^{18,20} A.Weber,¹ J.Weber,⁴⁶ R.Weill,²² C.Willmott,²⁵ F.Wittgenstein,¹⁷ D.Wright,³⁵ S.X.Wu,¹⁸ S.Wynhoff,¹ Z.Z.Xu,²⁰ B.Z.Yang,²⁰ C.G.Yang,⁶ G.Yang,¹⁸ X.Y.Yao,⁶ C.H.Ye,¹⁸ J.B.Ye,²⁰ Q.Ye,¹⁸ S.C.Yeh,⁴⁸ J.M.You,¹⁸ N.Yunus,¹⁸ M.Yzerman,² C.Zaccardelli,³² P.Zemp,⁴⁶ M.Zeng,¹⁸ Y.Zeng,¹⁸ D.H.Zhang,² Z.P.Zhang,^{20,18} B.Zhou,¹⁰ G.J.Zhou,⁶ J.F.Zhou,¹ R.Y.Zhu,³² A.Zichichi,^{8,17,18} B.C.C.van der Zwaan,²

-
- 1 I. Physikalisches Institut, RWTH, D-52056 Aachen, FRG[§]
 - III. Physikalisches Institut, RWTH, D-52056 Aachen, FRG[§]
 - 2 National Institute for High Energy Physics, NIKHEF, NL-1009 DB Amsterdam, The Netherlands
 - 3 University of Michigan, Ann Arbor, MI 48109, USA
 - 4 Laboratoire d'Annecy-le-Vieux de Physique des Particules, LAPP, IN2P3-CNRS, BP 110, F-74941 Annecy-le-Vieux CEDEX, France
 - 5 Johns Hopkins University, Baltimore, MD 21218, USA
 - 6 Institute of High Energy Physics, IHEP, 100039 Beijing, China
 - 7 Humboldt University, D-10099 Berlin, FRG
 - 8 INFN-Sezione di Bologna, I-40126 Bologna, Italy
 - 9 Tata Institute of Fundamental Research, Bombay 400 005, India
 - 10 Boston University, Boston, MA 02215, USA
 - 11 Northeastern University, Boston, MA 02115, USA
 - 12 Institute of Atomic Physics and University of Bucharest, R-76900 Bucharest, Romania
 - 13 Central Research Institute for Physics of the Hungarian Academy of Sciences, H-1525 Budapest 114, Hungary[‡]
 - 14 Harvard University, Cambridge, MA 02139, USA
 - 15 Massachusetts Institute of Technology, Cambridge, MA 02139, USA
 - 16 INFN Sezione di Firenze and University of Florence, I-50125 Florence, Italy
 - 17 European Laboratory for Particle Physics, CERN, CH-1211 Geneva 23, Switzerland
 - 18 World Laboratory, FBLJA Project, CH-1211 Geneva 23, Switzerland
 - 19 University of Geneva, CH-1211 Geneva 4, Switzerland
 - 20 Chinese University of Science and Technology, USTC, Hefei, Anhui 230 029, China
 - 21 SEFT, Research Institute for High Energy Physics, P.O. Box 9, SF-00014 Helsinki, Finland
 - 22 University of Lausanne, CH-1015 Lausanne, Switzerland
 - 23 Los Alamos National Laboratory, Los Alamos, NM 87544, USA
 - 24 Institut de Physique Nucléaire de Lyon, IN2P3-CNRS, Université Claude Bernard, F-69622 Villeurbanne Cedex, France
 - 25 Centro de Investigaciones Energeticas, Medioambientales y Tecnológicas, CIEMAT, E-28040 Madrid, Spain
 - 26 INFN-Sezione di Milano, I-20133 Milan, Italy
 - 27 Institute of Theoretical and Experimental Physics, ITEP, Moscow, Russia
 - 28 INFN-Sezione di Napoli and University of Naples, I-80125 Naples, Italy
 - 29 Department of Natural Sciences, University of Cyprus, Nicosia, Cyprus
 - 30 University of Nymegen and NIKHEF, NL-6525 ED Nymegen, The Netherlands
 - 31 Oak Ridge National Laboratory, Oak Ridge, TN 37831, USA
 - 32 California Institute of Technology, Pasadena, CA 91125, USA
 - 33 INFN-Sezione di Perugia and Università Degli Studi di Perugia, I-06100 Perugia, Italy
 - 34 Carnegie Mellon University, Pittsburgh, PA 15213, USA
 - 35 Princeton University, Princeton, NJ 08544, USA
 - 36 INFN-Sezione di Roma and University of Rome, "La Sapienza", I-00185 Rome, Italy
 - 37 Nuclear Physics Institute, St. Petersburg, Russia
 - 38 University of California, San Diego, CA 92093, USA
 - 39 Dept. de Física de Partículas Elementales, Univ. de Santiago, E-15706 Santiago de Compostela, Spain
 - 40 Bulgarian Academy of Sciences, Institute of Mechatronics, BU-1113 Sofia, Bulgaria
 - 41 Center for High Energy Physics, Korea Advanced Inst. of Sciences and Technology, 305-701 Taejon, Republic of Korea
 - 42 University of Alabama, Tuscaloosa, AL 35486, USA
 - 43 Purdue University, West Lafayette, IN 47907, USA
 - 44 Paul Scherrer Institut, PSI, CH-5232 Villigen, Switzerland
 - 45 DESY-Institut für Hochenergiephysik, D-15738 Zeuthen, FRG
 - 46 Eidgenössische Technische Hochschule, ETH Zürich, CH-8093 Zürich, Switzerland
 - 47 University of Hamburg, 22761 Hamburg, FRG
 - 48 High Energy Physics Group, Taiwan, China
- § Supported by the German Bundesministerium für Forschung und Technologie
‡ Supported by the Hungarian OTKA fund under contract number 2970.
‡ Also supported by CONICET and Universidad Nacional de La Plata, CC 67, 1900 La Plata, Argentina
† Deceased.

References

- [1] M. Perl *et al.*, Phys. Rev. Lett. **35** (1975) 1489.
- [2] For a comprehensive review see: K.G. Hayes in Particle Data Group, K. Hikasa *et al.*, Phys. Rev. **D 45** (1992) VI.19, and references therein.
- [3] W. Marciano, “Second Workshop on Tau Physics”, p. 502, edited by K.K. Gan, World Scientific, 1993.
- [4] L3 Collab., B. Adeva *et al.*, Nucl. Instr. and Meth. **A 289** (1990) 35.
- [5] S. Jadach, B.F.L. Ward and Z. Was, Comp. Phys. Comm. **66** (1991) 276.
- [6] The L3 detector simulation is based on GEANT Version 3.15, September 1989, see R. Brun *et al.*, “GEANT 3”, CERN DD/EE/84-1 (Revised), September 1987. Hadronic interactions are simulated based on the GHEISHA program; see H. Fesefeldt, RWTH Aachen PITHA 85/02 (1985).
- [7] L3 Collab., O. Adriani *et al.*, Phys. Lett. **B 294** (1992) 466;
- [8] V. Innocente, Y.F. Wang and Z.P. Zhang, Nucl. Instr. and Meth. **A 323** (1992) 647.
- [9] J. Hertz, A. Krogh and R.G. Palmer, “Introduction to the theory of neural computation”, Addison-Wesley, 1991.
P.D. Wasserman, “Neural computing, theory and practice”, Van Nostrand Reinhold, 1989.
- [10] L3 Collab., B. Adeva *et al.*, Z. Phys. **C 51** (1991) 179;
L3 Collab., M. Acciarri *et al.*, Z. Phys. **C 62** (1994) 551.
- [11] ARGUS Collab., H. Albrecht *et al.*, Z. Phys. **C 58** (1993) 61.
- [12] ARGUS Collab., H. Albrecht *et al.*, Phys. Lett. **B 260** (1991) 259.
- [13] A. Santocchia, Ph. D. Thesis, University of Perugia, 1994, unpublished.
- [14] HRS Collab., R. Tschirhart, *et al.*, Phys. Lett. **B 205** (1988) 407.
- [15] J. Urheim, “Second Workshop on Tau Lepton Physics”, p. 165, edited by K.K. Gan, World Scientific, 1993.
- [16] T. Skwarnicki, “Second Workshop on Tau Lepton Physics”, p. 217, edited by K.K. Gan, World Scientific, 1993.
CLEO Collab., M. Artuso *et al.*, CLNS 94/1281.
- [17] Particle Data Group, L. Montanet *et al.*, Phys. Rev. **D 50** (1994).
- [18] OPAL Collab., G. Alexander *et al.*, Phys. Lett. **B 266** (1991) 201;
OPAL Collab., R. Akers *et al.*, Phys. Lett. **B 328** (1994) 207.

Figure Captions

- Figure 1: The distribution of the number of neutral clusters in τ decays. The contributions of the various sources are indicated. Also shown is the case for five neutral clusters whose composition is determined from the branching ratios measured from events with four or fewer neutral clusters.
- Figure 2: The energy input variables to the neural networks. The contributions of the various sources are indicated. a) The energy distribution of π^\pm ; b) the energy distribution of neutral clusters; c) the distribution of the energy in the electromagnetic calorimeter transverse to the charged particle direction.
- Figure 3: The angular input variable to the neural networks in the sample of $h \rightarrow 2\pi^0$. The contributions of the various sources are indicated. a) The angle between the charged pion and the highest energy neutral cluster. b) The angle between the pion and the second highest energy neutral cluster. c) The angle between the highest and the second highest energy neutral clusters.
- Figure 4: The invariant mass distributions for selected events, assuming the π^\pm mass for charged clusters. The contributions of the various sources are indicated. The deviations in Fig. 4b and 4c may be result from slight imperfections in the simulation.

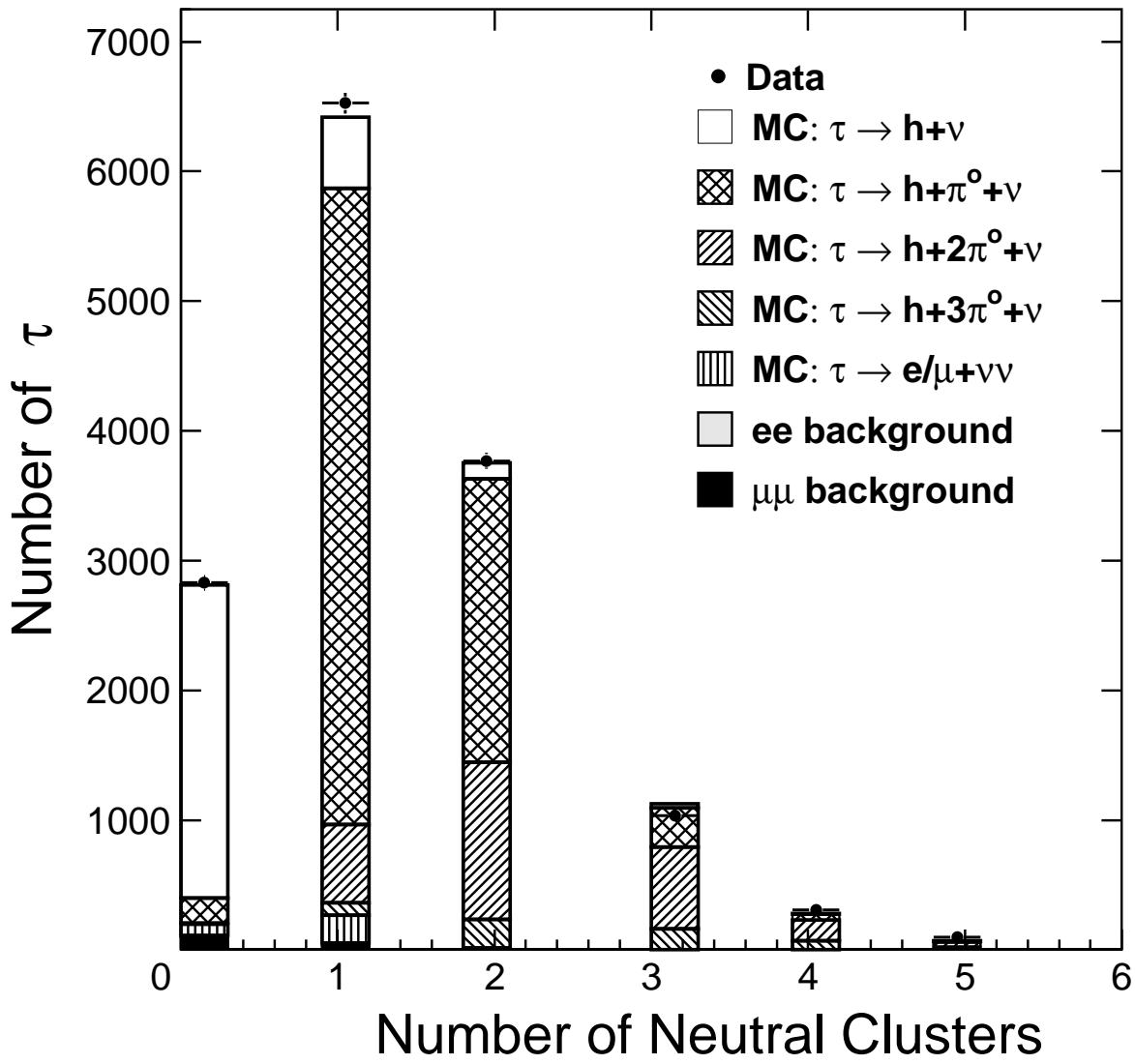


Figure 1

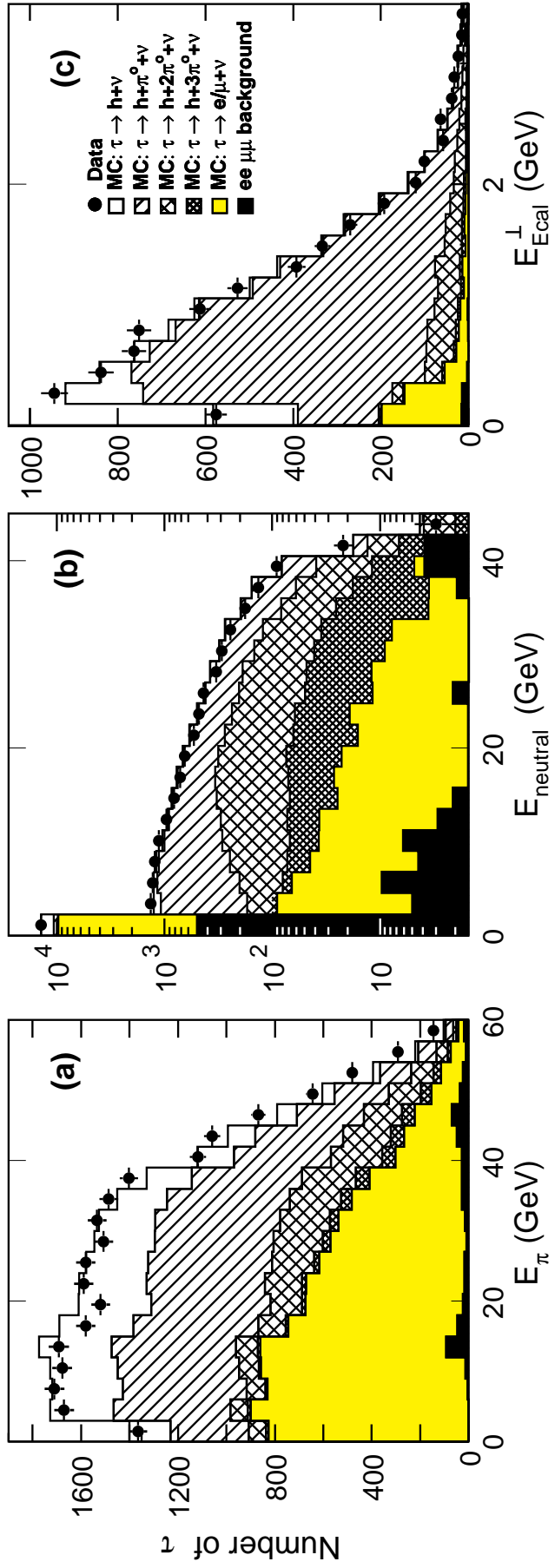


Figure 2

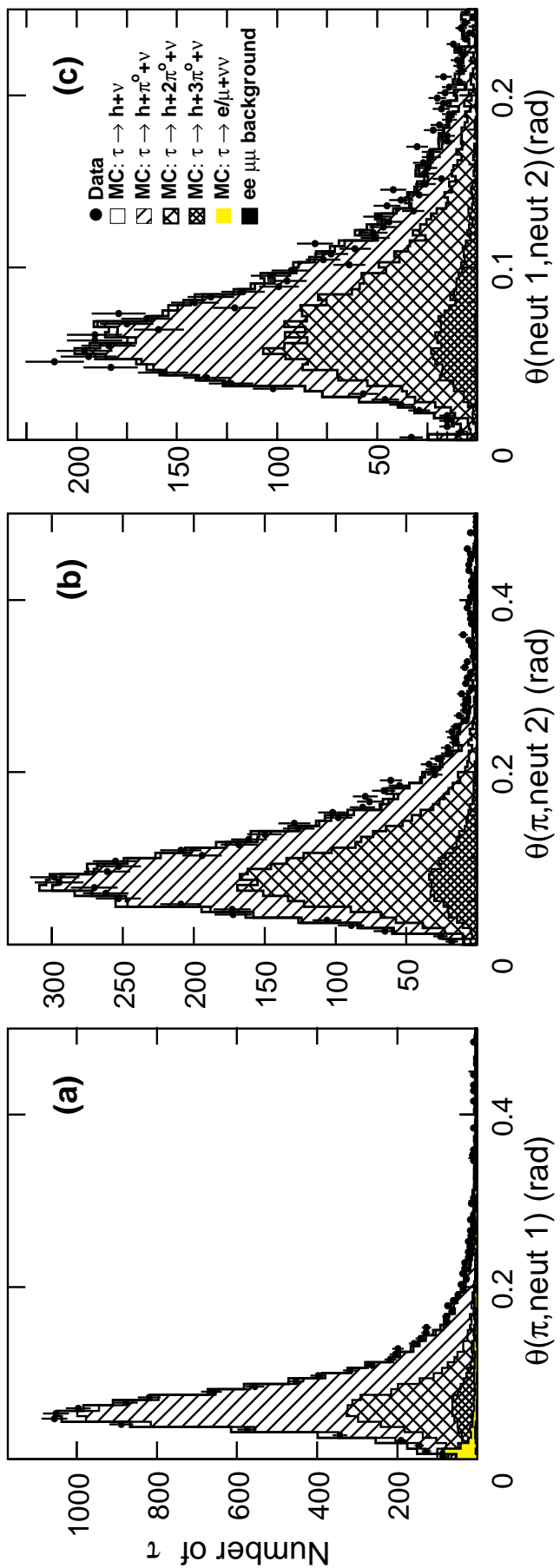


Figure 3

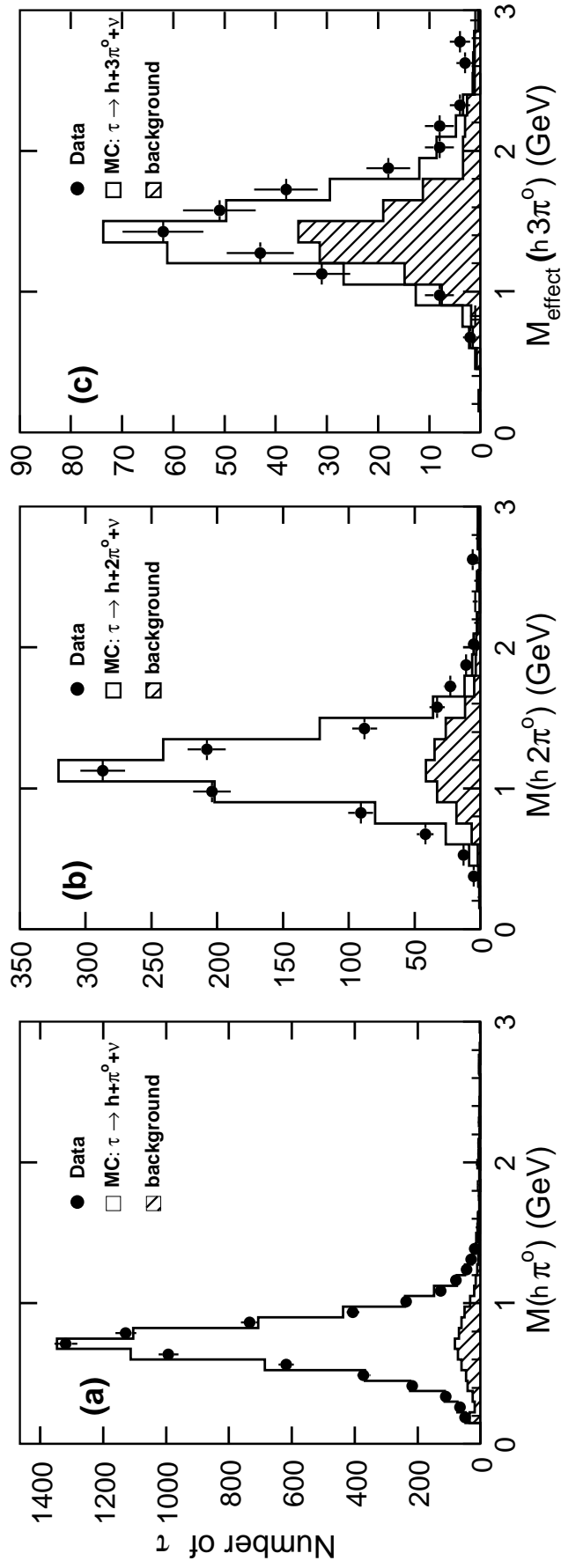


Figure 4